A biophysical model approach supporting the analysis of electrocardiograms during atrial fibrillation

Vincent Jacquemet[1], Adriaan van Oosterom[2],
Jean-Marc Vesin[1], Lukas Kappenberger[2]

1. *Signal Processing Institute, Ecole Polytechnique Fédérale de Lausanne (EPFL), CH-1015 Lausanne, Switzerland*
2. *Department of Cardiology, Centre Hospitalier Universitaire Vaudois (CHUV), CH-1011 Lausanne, Switzerland*

Published in IEEE Eng. Med. Biol. Mag. (2006), vol. 25, no. 6, pp. 79-88

Abstract

This paper describes how computer models of the atria can be used to assist the interpretation and the analysis of electrocardiograms (ECG) during atrial fibrillation (AF). Emphasis is put on the biophysical modeling of the active electric sources during normal rhythm, atrial flutter and AF, and of the passive body tissues that affect the amplitudes and waveforms of the signals as observed on the thorax. A comparison is presented between simulated and clinical ECGs, and inferences are drawn for the extraction of AF signals from the ECG and their subsequent analysis.

Keywords

Atrial fibrillation, computer modeling, electrocardiogram, forward problem, equivalent double layer

Introduction

Atrial fibrillation (AF) is the most frequently observed arrhythmia in the human heart. While it clearly causes discomfort in patients, it has long been believed to be relatively harmless and, unlike ventricular fibrillation, it is not immediately life threatening. However, of late it has become clear that AF often leads to severe complications such as heart failure and stroke [1, 2]. The presence of AF as such can easily be established by inspection of the standard electrocardiogram (ECG). During AF the electric wavelets arising from the atria appear in a chaotic manner, coinciding at times with those of the ventricles, the so-called QRST complexes. Conversely, in a normal situation, the atrial signals, here known as P waves, always directly precede the QRST waves.

AF can have different causes, ranging from viral infections to thyrotoxicosis. The present day classification is purely historically based and describes paroxysmal and chronic forms [3]. Invasive, electrophysiological studies [4] have identified one sub-form of AF as having its focal origin located in the region around the pulmonary veins. Current therapies for AF include: pharmaceutical therapy, electric cardio version (electric shock), catheter ablation along lines on the atrial endocardium and in extreme cases, surgical intervention.

The research discussed in this paper is motivated by the search for an optimal classification of the different types of AF on the basis of recorded atrial signals. This would facilitate the selection of an optimal therapy. The paper focuses on the biophysical modeling of the active electric sources during AF and of the passive body tissues that affect the amplitudes and waveforms of the signals as observed on the thorax. Some inferences for the analysis of AF signals that may be drawn from these models are highlighted.

Atrial Electrocardiograms

The standard 12-lead ECG is the most commonly used non-invasive tool for diagnosing cardiac electrically manifest abnormalities like that of arrhythmias. It represents simultaneously recorded electric signals, derived from nine electrodes placed on the thorax and on the extremities, as shown in Fig. 1B. The wave forms of the signals are

lead specific. An example of an ECG (lead V_1), recorded during a normal heart rhythm, is shown in the upper trace of Fig. 2. The PQRSTU nomenclature introduced by Einthoven [5] is indicated. In contrast, the lower trace of Fig. 2 shows the typical wave form observed in the lead V_1 in a patient during AF. Here the atrial activity is continuous, producing a signal with an irregular wave form that is superimposed on that of the ventricular signals. The ventricular heart rate is clearly more irregular than during sinus rhythm but is less irregular than that of the fibrillating atria owing to the fact that the electric trigger from atrial to ventricular tissue passes through, and is regulated by, a system of specialized cells: the atrio-ventricular node. The atrial signals are clearly much smaller (about 10 times) than those related to the ventricles (QRST complexes), both during normal rhythm (P waves) and arrhythmia (AF). As a consequence, the early diagnostic applications of the P wave forms were necessarily limited, and the use of the ECG during AF was mainly restricted to diagnosing AF as such.

In addition to ECG signals, the electrical activity of the atria can be recorded by passing catheter-guided electrodes through one of the major veins into the atria. The analysis of the recorded signals (endocardial electrograms), with their far greater detail, is used in diagnostic procedures as well as for guiding therapeutic interventions [6]. Advanced mapping procedures have been developed for scanning the electric activity on the atrial surface [7] or endocardium [8]. Such methods have led to the identification of different types of foci that trigger AF and the description of specific dynamics. Current basic research is aimed at linking these epi- or endocardial signals with different etiologies of the disease.

Recording conventional ECGs from the thorax clearly has a less invasive nature than a catheterization procedure. Moreover, the ECG provides a global, overall impression of the atrial activity, an impression that catheterization provides only through an elaborate, time-consuming procedure. However, an unfortunate consequence of the spreading out of the electric currents generated by the active atrial cells (myocytes) is that the electrical image that appears on the body surface is blurred. Another major complication is the fact that the (relatively much larger) signals arising from the electric activity of the ventricles are mixed with the atrial signals for a major part of the duration of a heart beat. This complication led to the development of different signal processing tools aimed at isolating the contribution of the atria to the ECG signals during AF, such

as QRST cancellation [9] and atrial/ventricular source separation [10]. The complete isolation of AF signals will open the way to the full extraction of their spatio-temporal information [11, 12].

Signal processing and feature extraction techniques applied to the ECG need to be validated in order to demonstrate their relevance for clinical applications. A common approach has been to apply the methods proposed to synthetic signals. For example, some features of the electrical activity of the atria during AF have been reproduced by a superposition of sine waves [9] or by combining rescaled P waves [13]. Primitive atrial signals were reconstructed from clinical ECGs by replacing the QT segments by weighted fibrillation waves extracted from the TQ interval [9]. A simple stochastic, 3-variable, dynamic system generating a sequence of QRST complexes has also been proposed [14]. In this paper we advocate the use of a more sophisticated signal generation, based on an electro-anatomical model of the atria and the application of volume conduction theory to the simulation of electrograms and ECGs. This approach is illustrated by showing some results derived through using a dedicated biophysical model that is being developed in our group. A comparison is presented between simulated and recorded signals, and inferences are drawn for the extraction of AF signals from the ECG and their subsequent analysis.

Electrical propagation in the atrial wall

Electrophysiological background

The contractile elements of the atria are located inside the myocytes: a structure of densely packed cells that form a muscle layer with a thickness of about 1-2 mm (Fig. 1A). All myocytes are activated by some (or all) of their direct neighbors. In turn, their activation assists in the activation of neighbors still at rest. In this manner a wave-like activation process is set up. Following activation, the cells gradually return to their resting state. During the first part of this recovery process, the so-called refractory period, the re-activation of the cells is impossible.

The activation and de-activation of the contractile elements is controlled by calcium ions (Ca^{2+}), the intracellular concentration of which is gated by the instantaneous potential difference across the cell membrane. This potential difference depends on the

concentrations of various other ions, in particular on those of sodium (Na^+) and potassium (K^+) ions. The gatekeepers of the associated fluxes of ions across the membrane have been localized in the cell membrane. These are the so-called ion channels, for which several different, ion-specific variants have been identified. The entire process of activation and recovery arises from the complex, dynamic interplay of these ions, fed by the underlying biochemical processes associated with the supply of the required contractile energy.

In the normal heart, activity starts in the right atrium at the position of the so-called sino-atrial node (SAN) (Fig. 1A). From there the activation process spreads out in a regular fashion over the atrial tissue (Fig. 3A) at a velocity of about 1 m/s. After recovery, the activation process is repeated only after a re-initiation in the sino-atrial node region.

Atrial fibrillation relates to the situation in which, continuously, parts of the myocardium are reactivated by wave fronts previously set up in the tissue. This requires the incoming wave front to arrive later than the local refractory period, a condition that is facilitated by any delay in the incoming wave front or by any reduction of the local refractory period. The complex geometry of the atria (Fig. 1A) provides various possibilities for these processes to form self-perpetuating processes around the orifices of the connecting vessels and those of the connections between the atria and the ventricles: the tricuspid and mitral valves. The condition of the wave anchoring around such orifices, setting up a periodic, but highly abnormal, activation pattern at an unusually high rate, is called atrial flutter (AFL). An example of the activation map during an episode of AFL is shown in Fig. 4A. Under some conditions, a completely irregular, chaotic type of activation is set off, *i.e.*, AF (Figs. 5A-D).

Modeling the normal activation process

As indicated above, the driving forces of the activation process are situated in, or near, the cell membrane. The activation sequence depends on the properties of the membrane kinetics, but also on the way the individual cells are electrically coupled to their direct neighbors. Mathematical modeling of the membrane kinetics has produced wave forms of transmembrane potentials that closely resemble those observed experimentally. Electrophysiological studies at the level of the membrane have provided

insight into the way various pharmaceutical interventions may influence membrane kinetics. Morphological studies have yielded detailed information on cell coupling. Different types of mathematical analysis have been presented of the conditions that give rise to fibrillatory, chaotic-like behavior of the entire system of highly nonlinear, coupled elements.

All factors listed above influence the propagation of the activation. The large number of myocytes involved (~2×10^8), the types of ions, ion-channels and their gating parameters, as well as the complex atrial anatomy prohibit the formulation of a fully comprehensive activation model. The computer models of electrical propagation in the atria that have recently been developed [15-23] differ in their accuracy of the representing electrophysiological and anatomical details. The specific modeling assumptions involved are motivated by the information available and justified by the specific research topic addressed.

Our current interest required an activation model capable of simulating normal activation, AF, and AFL. When applied to arrhythmia, the model should be flexible enough to test various hypotheses on the expression of the underlying etiology of the disease. The simulated epochs should be long enough to permit an appropriate statistical analysis of the activation patterns, which pose restraints on the model complexity in order to avoid a prohibitively long computing time. Furthermore, the model should exhibit a behavior compatible with that observed in invasive mapping studies of AF [7, 8].

The computer model of the human atria used in our study was based on a geometry derived from magnetic resonance images (MRI). This geometry includes the details of the entries and exits of the vessels as well as the locations of the valves connecting the atria to the ventricles [22, 24], which form natural barriers to the activation process. In addition, structures were added to model the crista terminalis, the pectinate muscles and Bachman's bundle. Their parameters were tuned to produce the (faster) propagation velocity of these tissues [17].

Inside the closed hull (Fig. 1A) encompassing all myocytes, with a mean wall thickness of 1.2-1.5 mm, the electric propagation of the cardiac impulse was derived by

solving, for all interior points $\vec{r}$ of the hull and for all time instances *t*, a reaction-diffusion system based on a detailed ionic model of the cell membrane kinetics. This approach entails solving the partial differential equation:

$$C_{\mathrm{m}} \frac{\partial V_{\mathrm{m}}}{\partial t} = S_{\mathrm{v}}^{-1} \nabla \cdot \sigma \nabla V_{\mathrm{m}} + I_{\mathrm{stim}} - I_{\mathrm{ion}} \ , \qquad (1)$$

where $V_{\mathrm{m}} = V_{\mathrm{m}}(\vec{r},t)$ represents the transmembrane potential, C_{m} the membrane capacitance (F m^{-2}), S_{v} the cell surface-to-volume ratio (m^{-1}), σ the electric conductivity tensor of the medium (S m^{-1}) and ∇ the vector of spatial derivatives. The system is driven by the ionic current density (A m^{-2}) generated near the membranes: $I_{\mathrm{ion}} = I_{\mathrm{ion}}(\vec{r},t)$, and, if the tissue is activated by an external stimulus, by the impressed current density (A m^{-2}): $I_{\mathrm{stim}} = I_{\mathrm{stim}}(\vec{r}_{\mathrm{stim}},t)$. The surface-to-volume ratio S_{v} represents the total area of cell membrane per unit of tissue volume. Equation (1) constitutes the so-called monodomain approximation of the bidomain formulation governing the propagation of the cardiac impulse in the myocardium [25].

The ion kinetics involved in our model for computing $I_{\mathrm{ion}}(\vec{r},t)$ is the one postulated by Courtemanche *et al*. for the human atrial myocyte [26]. It takes into account 12 different types of ionic channels, the variations in Ca^{2+}, Na^{+} and K^{+} intracellular concentrations, and the calcium dynamics in the sarcoplasmic reticulum. For each interior point of the atrial wall, a system of 21 coupled non-linear differential equations is solved by means of the forward Euler and the Rush-Larsen methods [27]. The standard parameter settings used in Eq. (1) are: C_m = 1 μF/cm^2, S_v = 0.24 μm^{-1}, σ = 0.56 S/m (uniform, isotropic) in the bulk of the tissue and σ = 1.2—2.0 S/m in the bundles. Equation (1) is solved numerically on a cubical grid in the interior of the atrial wall, using a finite difference approach [28], with time steps ranging from 12.5 to 50 μs adapted to the dynamical state of the ion kinetics [29]. The number of grid points involved is approximately 800,000. At the surface bounding the myocytes, the normal spatial derivative of the transmembrane potential is used as the boundary condition.

The model produces wave fronts propagating at conduction velocities of 75-120 cm/s during normal rhythm. The activation sequence at the grid points near the surface bounding the atrial myocardium resulting from a focus at the (natural) location of the

sino-atrial node is shown in Fig. 3A. The pattern is in agreement with what has been observed in electrophysiological mapping studies [30-32] and in other computer models [17]. The wave fronts are mainly oriented normal to the myocardial walls, their propagation being parallel to the walls.

Modeling the activation process during AFL

Typical AFL involves a macro-reentrant circuit around the superior and inferior vena cava with a line of functional block along the crista terminalis (the muscle bundle joining these veins). The wave front propagates counterclockwise (when observed from inside the atria) with an atrial rate ranging from 240 to 340 bpm for AFL type 1 [33]. Animal experiments and clinical data (see Waldo [33] for an overview) as well as computer models [17, 21, 34] have stressed the importance of anatomical structures (such as the crista terminalis) and slow conduction in the isthmus region for the initiation and the stability of AFL. Thus, the modeling of AFL requires both a membrane kinetics model capable of simulating reentries and functional blocks, and an anatomically correct geometry.

In our model, conditions set up in order to reproduce the reentrant activation pattern observed during AFL were as follows. The conduction properties were those used for the normal propagation, except in the isthmus between the inferior vena cava and the tricuspid valve, where the conduction velocity was reduced to 40 cm/s by decreasing the tissue conductivity, as in [17]. The action potential duration (APD) was also shortened to allow faster rates. Following the recommendation of Courtemanche *et al*. [35], the L-type Ca^{2+} current I_{CaL} and the outward K^+ currents I_{to}, I_{Kur}, I_{Kr} were selected as a target for these modifications. The channel conductances associated with the ionic currents I_{to}, I_{CaL}, I_{Kur}, I_{Kr} were altered by factors 0.2, 0.5, 0.1, 2.5 respectively, resulting in an APD_{90} (measured at 90% repolarization) of 150 ms. AFL initiation was performed through a S_1-S_2 stimulation protocol (a normal beat followed by a premature beat initiated in the isthmus) and imposing a line of block in the isthmus region. The resulting activation sequence during simulated AFL is presented in Fig. 4A. The atrial rate is about 310 bpm.

Modeling the activation process during AF

While different mapping techniques have provided significant information on the electrophysiological processes associated with AF [7, 36], the mechanisms underlying its initiation and maintenance remain unclear. Several conceptual descriptions of AF have been proposed. According to the multiple wavelets hypothesis, AF perpetuation relies on several wavelets randomly propagating over the atria and undergoing fractionation, coalescence and collisions through a turbulence process ensuring the maintenance of a sufficient number of wavelets [7, 37]. More recently, evidences of spatio-temporal organization in experimental models of AF suggested another mechanism, the mother rotor hypothesis, postulating that a single source (or possibly a small number of sources) of reentrant wave fronts, maintains the fibrillatory activity [4, 36, 38]. Maybe both mechanisms are involved. In this debate, computer models can provide new insights by exhibiting idealized models of AF in which the mechanisms can be clearly identified [20, 22, 39, 40]. Here, to illustrate the potential of modeling, a computer model of AF inspired by the work of Fareh *et al*. [41] is presented, in which the perpetuation of AF is ensured by the presence of heterogeneities in APD.

In order to create a substrate for AF, patchy heterogeneities (spatial scale: 2 cm) in APD_{90} were introduced by modifying the local membrane properties. The channel conductances associated with the ionic currents I_{to}, I_{CaL}, I_{Kur}, I_{Kr} were altered by factors 0.2, 0.7, 0.1, 1.5 (respectively) in the patches and by factors 3, 0.5, 1, 3 elsewhere. This resulted in an APD_{90} distribution of 195±15 ms (range: 150-230 ms) during normal rhythm [39]. Next, sustained AF was induced by rapid pacing (cycle length: 150 ms) during 11 seconds applied to the appendage of the left atrium. The pacing site was located in a region with short APD_{90}, close to a large gradient in refractoriness, as in the dog study by Fareh *et al*. [41]. Simulated AF was observed as 3 to 6 wave fronts propagating and interacting over the atria with a wavelength of 7.6±1.2 cm, and undergoing wave breaks at the location of large gradients in refractoriness [39]. This wavelet dynamics is illustrated in Figs. 5A-D.

From Atrial Activity to Potentials

Equivalent source descriptions

During the activation and repolarization of the myocytes, electric currents flow from each cell to its direct neighbors. The return currents flow through the extracellular myocardial space and a fraction of it passes into the medium outside the myocardium, setting up potential differences in the surrounding, electrically passive tissues. According to the bidomain theory in its monodomain approximation [25, 42], the equivalent electric sources resulting from the membrane activity at locations $\vec{r}$ throughout the myocardium are

$$I_{\mathrm{m}}(\vec{r},t) = \sigma_{\mathrm{i}} \nabla^2 V_{\mathrm{m}}(\vec{r},t)) \,, \tag{2}$$

where σ_{i} is the electric conductivity of the intracellular domain, with $I_{\mathrm{m}}(\vec{r},t)$ having the nature of an impressed current source volume density (A m^{-3}), and $V_{\mathrm{m}}(\vec{r},t)$ as found by solving Eq. (1). These sources feed currents into the extracellular domain. In a volume conductor with conductivity σ_{e} , the potential in the extracellular space, $\Phi(\vec{y},t)$, follows from the impressed electric current sources I_{m} by solving the differential equation [43]

$$\sigma_{\mathrm{e}} \nabla^2 \, \Phi(\vec{y},t) = I_{\mathrm{m}}(\vec{x},t) \,, \tag{3}$$

which expresses the conservation of current. For reasons of clarity, $\vec{y}$ and $\vec{x}$ are used to denote the position of the field point and the source location, respectively. In the bidomain approach, for any point inside the myocardial wall we have: $\vec{y} = \vec{x} = \vec{r}$, and for a field point outside the myocardium,

$$\sigma_o \nabla^2 \, \Phi(\vec{y},t) = 0 \,, \tag{4}$$

with σ_0 the conductivity of the medium outside the heart. The potentials outside the heart may now be found by using the boundary element method (BEM) [44]. This permits the computation of the potential distribution throughout the body, modeled by a piecewise homogenous volume conductor. A conceptually important first step in this method is the computation of the so-called infinite medium potential, *i.e.* the potential field in the outside domain generated by the sources when placed inside a medium of infinite extent and homogeneous conductivity. When taking $\sigma_0 = \sigma_e$, the infinite medium potential solution to Eqs. (3) and (4), after substitution of Eq. (2), is

$$\Phi_\infty(\vec{y},t) = \frac{\sigma_\mathrm{i}}{4\pi\sigma_e}\int_\mathrm{V}\frac{\nabla^2 V_\mathrm{m}(\vec{x},t)}{r}\,\mathrm{d}v\,, \tag{5}$$

with r the length of the vector $\vec{r}$ from any source location source $\vec{x}$ to field point $\vec{y}$. The integral in Eq. (5) is taken over all active sources within the entire atrial myocardium. In spite of its simplicity this equation is not very practical when determining (and analyzing) the elementary contributions generated by all of the (800,000) computed transmembrane potentials. The following, alternative expression was formulated by Geselowitz [43, 45], who derived it by applying some classic results from field theory. It reads

$$\Phi_\infty(\vec{y},t) = \frac{-\sigma_\mathrm{i}}{4\pi\sigma_o}\int_\mathrm{S} V_\mathrm{m}(\vec{x},t)\,\mathrm{d}\omega\,, \tag{6}$$

with $\mathrm{d}\omega = \mathrm{d}\omega(\vec{y},\vec{x})$ the solid angle subtended by a surface element around point $\vec{x}$ on the surface S bounding all atrial myocytes (endocardium and epicardium) at field point $\vec{y}$. This expression holds true for the monodomain approximation, provided the conductivity σ_i is taken to be uniform.

In Eq. (6), the transmembrane potentials near the atrial surface act as the strength of an equivalent double layer (EDL). The potentials computed at the grid points of the atrial model close to the bounding surface acted as the EDL strength. The conductivity ratio $\sigma_\mathrm{i}/\sigma_e$ was set to 1/3, resulting in a maximal effective source strength (during the upstroke of the transmembrane potential) of about 40 mV, as used in previous studies.

Accounting for volume conductor effects

The geometry of a healthy subject was documented by MRI methods [44]. The MR images were used to extract the geometry of the heart, lungs and torso, as well as of the ventricular cavities. To this ventricular geometry, tested extensively in previous studies, the geometry of the atrial model (Fig. 1A) was fitted, by means of translation, rotation and scaling. The atrial cavities were connected to the corresponding ventricular ones. These cavities constitute the major elements of modeling the electric volume conductor effects inside the thorax. The conductivity σ_o was set to 0.2 S/m in the torso and in the myocardium, to 0.6 S/m in the blood filled cavities and to 0.04 S/m in the lungs, and was assumed to be homogeneous and isotropic inside each of the compartments [46].

Finally, the potentials at all conductivity interfaces were computed by means of dedicated BEM software, developed during previous studies [44]. A major asset of the BEM is that the effect of the bounded conductivity at the torso surface and of the inhomogeneities may be computed independently of the instantaneous source strength. This can be viewed as an operator (matrix) acting on a vector representing the infinite medium potentials for all different types of atrial activity computed by using Eq. (5).

Although the assumptions listed for the EDL source may not always entirely hold true, its adoption to represent the cardiac sources of myocytes throughout the entire cardiac cycle has proved to be a very useful approximation, both for the ventricular [47] and the atrial activity [46].

The forward formulation

In the two preceding sections, the two major aspects of the genesis of atrial signals were described: the source model and the volume conductor model (Fig. 6). The results of each of these steps may be expressed by means of matrices: the sources by a matrix **S**, whose elements $s_{n,t}$ express the source (EDL) strength of node *n* of the atrial surface at time instant *t*, and a transfer matrix **A** with $a_{\ell,n}$ the potential generated at observation point ℓ (lead position) by a unit strength source element at node *n*:

$$\mathbf{\Phi = A\ S}\ . \qquad (7)$$

The boundary element method permits the computation of the potentials at any observation point inside the thorax. Observation points on the atrial surface result in electrograms, those on the torso surface result in ECGs. This requires merely that such points be defined on surfaces involved in the computation of **A**.

Simulated potentials

The forward formulation Eq. (7) was applied to the atrial sources as computed for normal atrial activation (Fig. 3), atrial flutter (Fig. 4) and atrial fibrillation (Fig. 5). The resulting, corresponding potentials are shown in the lower panels of these figures.

Figure 3B shows the simulated P waves superimposed on the ones measured on the healthy subject studied. In Fig. 3C these signals have been combined with the corresponding result for the ventricular depolarization and repolarization as obtained previously [44, 47, 48]. The similarity of measured and simulated data for the atrial signals is poorer than that for the ventricular ones. We attribute this to the fact that the atrial geometry is an approximate one. However, both amplitude and general wave form of the simulated P waves were recaptured correctly, not only for the signals of the standard leads, but in fact for all of the 64 leads for which the ECGs had been recorded [44].

The simulated AFL signals in the standard 12-leads, corresponding to the activation pattern of Fig. 4A, are shown in Fig. 4B. Since no clinically evaluated reference signals for this particular pattern were available, the recorded AFL signals shown in Fig. 4C merely support the correctness of the overall amplitude level of the signals as well as of their rate.

The simulated AF signals as shown in Fig. 5E cannot be evaluated rigorously since no clinical data was available for the (healthy) subject studied. However, the signals shown in Fig. 5F, recorded in a patient, clearly exhibit the same amplitude, and have a similar spatio-temporal appearance. Note that a method for reducing the QRST involvement was applied.

Applications

The atrial model was evaluated in several different ways [15, 22, 24], as were the methods for treating the volume conduction effects [46-49]. In combination with the results shown in Figs. 3-5, we felt confident that the models of atrial activity and volume conduction effects would be helpful in establishing possibilities and limitations of the methods for the characterization of AF on the basis of recorded ECGs. Here some applications to related, basic signal analytical problems are presented.

Spectral analysis

The complex dynamics of the activation process during AF (Figs. 5A-D) is reflected in transmembrane potentials (TMP). In Fig. 7 (upper trace) the time course of the

transmembrane potential of one of the nodes of the atrial model is shown. It acts as the strength for one of the (1300) elementary EDL sources of our model, the one closest to the position of the electrode recording V_1. The potentials in the extracellular domain generated by all of these source elements, as computed by using Eq. (7), is depicted by the electrogram at the node (middle trace) and by the ECG signal of lead V_1 (lower trace). Whereas the timing of the upstroke of the TMP is clearly visible in the electrogram, the signal shown in lead V_1 is more diffuse. This results of course from the addition of the contributions of all source elements.

The model permits the inspection of such signals “uncontaminated” by ventricular (QRST) involvement or different instrumental artifacts. One of the ways to characterize AF is by spectral analysis applied to ECG data. The model permits us to perform a similar type of analysis applied to the source data. The atrial electrograms were simulated at all 1300 source nodes. For each node, the number of depolarizations within a period of 25 s was documented. This specified a mean ‘firing’ rate at each node [24]. The spatial distribution of the intrinsic effective refractory period induced node-to-node variations in mean rates. The histogram of these rates is shown in Fig. 8B. In addition, a principal component analysis was performed on the standard lead signals. The power spectral density of the dominant (first) principal signal component is depicted in Fig. 8A. By comparing Fig. 8A with Fig. 8B it can be seen that the spectrum observed at the body surface resembles a blurred version of the rate histogram. However, the locations of the two peaks of this bimodal spectrum can be established.

QRST cancellation

As shown above, the models presented in this paper allow us to simulate realistic atrial ECG signals (Figs. 3-5) as well as ventricular signals in one and the same realistic model of the thorax, with the required level of detail in volume conduction aspects. The potentials may be, and have in fact been, computed in any of the 300 points specifying the torso surface. This offers the possibility of studying the full performance of spatio-temporal methods for reducing the ventricular involvement in AF signals. Specifically, the atrial (AF) signals and the QRST signals may be computed independently. The sum of these components may then be used in any cancellation procedure to be tested, with the simulated AF components serving as the gold standard.

Lead systems for studying AF

Based on the history of the standard 12-lead ECG, the location of its nine electrodes (Fig. 1B) can hardly be presumed to be optimal. As mentioned before, the early application of the ECG concentrated on the analysis of ventricular activity. Clearly, as is done in Body Surface Potential Mapping (BSPM) procedures, the inclusion of a much larger number of electrodes (in BSPM 24 to 220 [50]) would reduce the risk of relevant information available in the ECG being missed. However large a number of electrodes one may want to apply, the question that always remains is of where to place them most optimally. Moreover, this question requires to be answered in the context of the disease studied [51, 52].

For AF, the problem in hand is illustrated in Fig. 9. In Panel C, simulated AF signals are shown for the standard 12-lead ECG. Since just 9 electrodes are involved, the number of independent signal components is at most 8. As can be seen, the wave forms of leads V_4-V_6 are very similar, and, hence, these signals are highly correlated. Moreover, the wave form of lead V_R is, apart from its sign, also very close to those of leads V_4-V_6. This must mean that the information on AF as obtained by using the standard positions of the 9 electrodes must be sub-optimal. But, if just 9 electrodes were to be placed, where would that be? The types of models presented in this paper may be used in the answering of this question. A matrix of the correlation coefficients of all simulated AF signals at all 300 lead positions on the model of the thorax was computed, based on the signals during a time interval of 1 s (subset shown in Fig. 9C). The values (correlation coefficients) of any row (or column) of this symmetric matrix may be depicted by a map drawn on the torso surface. Fig. 9B displays just such a map for lead V_4. Note that the region close to lead V4 exhibits high positive correlation coefficients, and that indeed, V_R is strongly, negatively, correlated. So where, on the basis of this map, would one place an additional electrode? Since we are aiming for additional information this could be anywhere along the line showing zero correlation, but where? Clearly, V_1 lies along this line, and may remain included. If we now move to the location of V_1, its correlation map (Fig. 9A) may yield new, possible positions for additional information. Figure 9A now identifies locations superior to those of V_1 and V_2 as new candidates, which is not unlikely in view of the geometry shown in Fig. 1B.

The above discussion is merely included to illustrate the fact that the standard 12 leads are sub-optimal. Better methods for finding optimal lead positions are available, and are being currently explored in our group, facilitated by the biophysical models described in this paper.

Inverse solutions in AF?

The models described in this paper led to the formulation of Eq. (7). This represents what is known as a forward formulation (Fig. 6). On the basis of an assumed source description (transmembrane potentials on the surface bounding the atria) and a specific volume conductor model (piecewise inhomogeneous, isotropic sub regions: lungs and cavities), potentials are computed on the thorax. The realism and quality of the simulated potentials depends on the realism of the various applied, or implied, modeling assumptions, and the ones used here seem to be adequate.

The corresponding inverse procedure would aim at computing the parameters of the source model on the basis of potentials observed on the thorax (Fig. 6). For a single propagated beat, initiated at a single focus, this has indeed been shown to be possible; for the ventricles (see, e.g., [53]), and, more recently, for the atria (see, e.g., [46, 54]). However, in AF the situation is different. The observed signals have a chaotic-like appearance, and spatio-temporal constraints, required to safeguard the realism of the solutions [55], are not readily available. It is here that one may have to rely on signal analytical methods. An example of this is shown in Fig. 8, and the models of the type presented in this paper may help to develop the required preprocessing steps and to identify suitable signal parameters that can be interpreted in terms of specific types of AF.

Conclusion

Biophysical models of the genesis of ECG waveforms during AF were described. The model of the electric activity of the atria was found to have sufficient realism to be used to describe the electric sources during AF. The inclusion of the volume conduction model resulted in electrocardiographic signals that are in all aspects similar to those observed clinically. The model is currently applied to solve various problems related to optimal signal preprocessing and extraction of features in AF signals for the classification of AF

abnormalities. The biophysical model of the atrial activity is an essential element in this research, since it is capable of describing the electric source specifications derived from different hypotheses relating to the etiology of AF.

Acknowledgment

The authors wish to thank Dr. A. Forclaz for providing the clinical AF signals (Figs. 2, 4C, 5F), acquired in the course of an ongoing research project. Ryan Lahm, Josée Morisette and Arthur Stillman (Medtronic Inc) kindly furnished the MRI data for modeling the atrial geometry.

The study was made possible by grants from the Theo Rossi Di Montelera Foundation, Medtronic Europe, the Swiss Governmental Commission of Innovative Technologies (CTI), and the Swiss National Science Foundation (SNSF).

References

[1] E. N. Prystowsky, D. W. Benson, Jr., V. Fuster, R. G. Hart, G. N. Kay, R. J. Myerburg, G. V. Naccarelli, and D. G. Wyse, "Management of patients with atrial fibrillation. A Statement for Healthcare Professionals. From the Subcommittee on Electrocardiography and Electrophysiology, American Heart Association," *Circulation*, vol. 93, pp. 1262-77, 1996.

[2] R. Ruffy, "Atrial fibrillation," in *Cardiac electrophysiology: from cell to bedside*, J. Jalife and D. P. Zipes, Eds. Philadelphia: W. B. Saunders, 2000, pp. 682-690.

[3] V. Fuster, L. E. Ryden, R. W. Asinger, D. S. Cannom, H. J. Crijns, R. L. Frye, J. L. Halperin, G. N. Kay, W. W. Klein, S. Levy, R. L. McNamara, E. N. Prystowsky, L. S. Wann, and D. G. Wyse, "ACC/AHA/ESC guidelines for the management of patients with atrial fibrillation. A report of the American College of Cardiology/American Heart Association Task Force on Practice Guidelines and the European Society of Cardiology Committee for Practice Guidelines and Policy Conferences (Committee to develop guidelines for the management of patients with atrial fibrillation) developed in collaboration with the North American Society of Pacing and Electrophysiology," *Eur Heart J*, vol. 22, pp. 1852-923, 2001.

[4] M. Haissaguerre, P. Jais, D. C. Shah, A. Takahashi, M. Hocini, G. Quiniou, S. Garrigue, A. Le Mouroux, P. Le Metayer, and J. Clementy, "Spontaneous initiation of atrial

fibrillation by ectopic beats originating in the pulmonary veins," *N Engl J Med*, vol. 339, pp. 659-66, 1998.

[5] W. Einthoven and K. de Lint, "Ueber das normale menschliche Elektrokardiogram und die capillar-elektrometrische Untersuchung einiger Herzkranken," *Pflugers Arch Gesamte Physiol Menschen Tiere*, vol. 80, pp. 139-160, 1900.

[6] V. Barbaro, P. Bartolini, G. Calcagnini, and F. Censi, "Extraction of physiological and clinical information from intra-atrial electrograms during atrial fibrillation: review of methods," *Ann Ist Super Sanita*, vol. 37, pp. 319-24, 2001.

[7] K. T. Konings, C. J. Kirchhof, J. R. Smeets, H. J. Wellens, O. C. Penn, and M. A. Allessie, "High-density mapping of electrically induced atrial fibrillation in humans," *Circulation*, vol. 89, pp. 1665-80, 1994.

[8] S. Shpun, L. Gepstein, G. Hayam, and S. A. Ben-Haim, "Guidance of radiofrequency endocardial ablation with real-time three-dimensional magnetic navigation system," *Circulation*, vol. 96, pp. 2016-21, 1997.

[9] M. Stridh and L. Sornmo, "Spatiotemporal QRST cancellation techniques for analysis of atrial fibrillation," *IEEE Trans Biomed Eng*, vol. 48, pp. 105-11, 2001.

[10] F. Castells, J. J. Rieta, J. Millet, and V. Zarzoso, "Spatiotemporal blind source separation approach to atrial activity estimation in atrial tachyarrhythmias," *IEEE Trans Biomed Eng*, vol. 52, pp. 258-67, 2005.

[11] M. Stridh, L. Sornmo, C. J. Meurling, and S. B. Olsson, "Sequential characterization of atrial tachyarrhythmias based on ECG time-frequency analysis," *IEEE Trans Biomed Eng*, vol. 51, pp. 100-14, 2004.

[12] A. Bollmann, D. Husser, M. Stridh, L. Soernmo, M. Majic, H. U. Klein, and S. B. Olsson, "Frequency measures obtained from the surface electrocardiogram in atrial fibrillation research and clinical decision-making," *J Cardiovasc Electrophysiol*, vol. 14, pp. S154-61, 2003.

[13] J. Healey, G. D. Clifford, L. Kontothanassis, and P. E. McSharry, "An open-source method for simulating atrial fibrillation using ECGSYN," *Computers in Cardiology*, vol. 31, pp. 425-7, 2004.

[14] P. E. McSharry, G. D. Clifford, L. Tarassenko, and L. A. Smith, "A dynamical model for generating synthetic electrocardiogram signals," *IEEE Trans Biomed Eng*, vol. 50, pp. 289-94, 2003.

[15] O. Blanc, N. Virag, J. M. Vesin, and L. Kappenberger, "A computer model of human atria with reasonable computation load and realistic anatomical properties," *IEEE Trans Biomed Eng*, vol. 48, pp. 1229-37, 2001.

[16] R. A. Gray and J. Jalife, "Ventricular fibrillation and atrial fibrillation are two different beasts," *Chaos*, vol. 8, pp. 65-78, 1998.

[17] D. Harrild and C. Henriquez, "A computer model of normal conduction in the human atria," *Circ Res*, vol. 87, pp. E25-36, 2000.

[18] C. J. Kafer, "Internodal pathways in the human atria: a model study," *Comput Biomed Res*, vol. 24, pp. 549-63, 1991.

[19] E. Macchi, "Digital-computer simulation of the atrial electrical excitation cycle in man," *Adv Cardiol*, vol. 10, pp. 102-110, 1974.

[20] G. K. Moe, W. C. Rheinboldt, and J. A. Abildskov, "A Computer Model Of Atrial Fibrillation," *Am Heart J*, vol. 67, pp. 200-20, 1964.

[21] E. J. Vigmond, R. Ruckdeschel, and N. Trayanova, "Reentry in a morphologically realistic atrial model," *J Cardiovasc Electrophysiol*, vol. 12, pp. 1046-54, 2001.

[22] N. Virag, V. Jacquemet, C. S. Henriquez, S. Zozor, O. Blanc, J. M. Vesin, E. Pruvot, and L. Kappenberger, "Study of atrial arrhythmias in a computer model based on magnetic resonance images of human atria," *Chaos*, vol. 12, pp. 754-763, 2002.

[23] C. W. Zemlin, H. Herzel, S. Y. Ho, and A. Panfilov, "A realistic and efficient model of excitation propagation in the human atria," in *Computer simulation and experimental assessment of cardiac electrophysiology*, N. Virag, O. Blanc, and L. Kappenberger, Eds. Armonk, New York: Futura Publishing, 2001, pp. 29-34.

[24] V. Jacquemet, N. Virag, Z. Ihara, L. Dang, O. Blanc, S. Zozor, J. M. Vesin, L. Kappenberger, and C. Henriquez, "Study of unipolar electrogram morphology in a computer model of atrial fibrillation," *J Cardiovasc Electrophysiol*, vol. 14, pp. S172-9, 2003.

[25] C. S. Henriquez and A. A. Papazoglou, "Using computer models to understand the roles of tissue structure and membrane dynamics in arrhythmogenesis," *Proc. IEEE*, vol. 84, pp. 334-354, 1996.

[26] M. Courtemanche, R. J. Ramirez, and S. Nattel, "Ionic mechanisms underlying human atrial action potential properties: insights from a mathematical model," *Am J Physiol*, vol. 275, pp. H301-21, 1998.

[27] S. Rush and H. Larsen, "A practical algorithm for solving dynamic membrane equations," *IEEE Trans Biomed Eng*, vol. 25, pp. 389-92, 1978.

[28] F. Fenton and A. Karma, "Vortex dynamics in three-dimensional continuous myocardium with fiber rotation: Filament instability and fibrillation," *Chaos*, vol. 8, pp. 20-47, 1998.

[29] Z. Qu and A. Garfinkel, "An advanced algorithm for solving partial differential equation in cardiac conduction," *IEEE Trans Biomed Eng*, vol. 46, pp. 1166-8, 1999.

[30] J. L. Cox, T. E. Canavan, R. B. Schuessler, M. E. Cain, B. D. Lindsay, C. Stone, P. K. Smith, P. B. Corr, and J. P. Boineau, "The surgical treatment of atrial fibrillation. II. Intraoperative electrophysiologic mapping and description of the electrophysiologic basis

of atrial flutter and atrial fibrillation," *J Thorac Cardiovasc Surg*, vol. 101, pp. 406-26, 1991.

[31] R. De Ponti, S. Y. Ho, J. A. Salerno-Uriarte, M. Tritto, and G. Spadacini, "Electroanatomic analysis of sinus impulse propagation in normal human atria," *J Cardiovasc Electrophysiol*, vol. 13, pp. 1-10, 2002.

[32] M. D. Rodefeld, B. H. Branham, R. B. Schuessler, D. E. Hand, C. M. Gamache, J. W. Platt, S. P. Labarbera, J. L. Cox, and J. P. Boineau, "Global electrophysiological mapping of the atrium: computerized three-dimensional mapping system," *Pacing Clin Electrophysiol*, vol. 20, pp. 2227-36, 1997.

[33] A. L. Waldo, *Atrial flutter: from mechanism to treatment*, vol. 14. Armonk, NY: Futura Publishing Company, Inc., 2001.

[34] W. S. Ellis, A. SippensGroenewegen, D. M. Auslander, and M. D. Lesh, "The role of the crista terminalis in atrial flutter and fibrillation: a computer modeling study," *Ann Biomed Eng*, vol. 28, pp. 742-54, 2000.

[35] M. Courtemanche, R. J. Ramirez, and S. Nattel, "Ionic targets for drug therapy and atrial fibrillation-induced electrical remodeling: insights from a mathematical model," *Cardiovasc Res*, vol. 42, pp. 477-89, 1999.

[36] J. Chen, R. Mandapati, O. Berenfeld, A. C. Skanes, R. A. Gray, and J. Jalife, "Dynamics of wavelets and their role in atrial fibrillation in the isolated sheep heart," *Cardiovasc Res*, vol. 48, pp. 220-32, 2000.

[37] G. K. Moe, "On the multiple wavelet hypothesis of atrial fibrillation," *Arch Int Pharmacodyn Ther*, vol. 140, pp. 183-188, 1962.

[38] A. C. Skanes, R. Mandapati, O. Berenfeld, J. M. Davidenko, and J. Jalife, "Spatiotemporal periodicity during atrial fibrillation in the isolated sheep heart," *Circulation*, vol. 98, pp. 1236-48, 1998.

[39] V. Jacquemet, N. Virag, and L. Kappenberger, "Wavelength and vulnerability to atrial fibrillation: insights from a computer model of human atria," *Europace*, vol. 7, pp. S83-92, 2005.

[40] J. Kneller, R. Zou, E. J. Vigmond, Z. Wang, L. J. Leon, and S. Nattel, "Cholinergic atrial fibrillation in a computer model of a two-dimensional sheet of canine atrial cells with realistic ionic properties," *Circ Res*, vol. 90, pp. E73-87, 2002.

[41] S. Fareh, C. Villemaire, and S. Nattel, "Importance of refractoriness heterogeneity in the enhanced vulnerability to atrial fibrillation induction caused by tachycardia-induced atrial electrical remodeling," *Circulation*, vol. 98, pp. 2202-9, 1998.

[42] R. M. Gulrajani, *Bioelectricity and Biomagnetism*: John Wiley & Sons, 1998.

[43] D. B. Geselowitz, "On the theory of the electrocardiogram," *Proc. IEEE*, vol. 77, pp. 857-876, 1989.

[44] G. Huiskamp and A. Van Oosterom, "The depolarization sequence of the human heart surface computed from measured body surface potentials," *IEEE Trans Biomed Eng*, vol. 35, pp. 1047-58, 1988.

[45] D. B. Geselowitz, "Description of cardiac sources in anisotropic cardiac muscle. Application of bidomain model," *J Electrocardiol*, vol. 25 Suppl, pp. 65-7, 1992.

[46] A. van Oosterom and V. Jacquemet, "Genesis of the P wave: atrial signals as generated by the equivalent double layer source model," *Europace*, vol. 7, pp. S21-29, 2005.

[47] A. van Oosterom, "Genesis of the T wave as based on an equivalent surface source model," *J Electrocardiol*, vol. 34 Suppl, pp. 217-27, 2001.

[48] A. van Oosterom and T. F. Oostendorp, "ECGSIM: an interactive tool for studying the genesis of QRST waveforms," *Heart*, vol. 90, pp. 165-8, 2004.

[49] G. Huiskamp, "Simulation of depolarization in a membrane-equations-based model of the anisotropic ventricle," *IEEE Trans Biomed Eng*, vol. 45, pp. 847-55, 1998.

[50] R. Hoekema, G. Uijen, and A. van Oosterom, "The number of independent signals in body surface maps," *Methods Inf Med*, vol. 38, pp. 119-24, 1999.

[51] F. Kornreich, M. Kavadias, T. J. Montague, P. M. Rautaharju, and M. B. Horacek, "Selection of optimal electrocardiographic leads from body surface potential maps for the diagnosis of left ventricular hypertrophy," in *Electrocardiology'88*, H. Abel, Ed.: Elsevier Science, Amsterdam, 1989, pp. 329-32.

[52] F. Kornreich, T. J. Montague, P. M. Rautaharju, P. Block, J. W. Warren, and M. B. Horacek, "Identification of best electrocardiographic leads for diagnosing anterior and inferior myocardial infarction by statistical analysis of body surface potential maps," *Am J Cardiol*, vol. 58, pp. 863-71, 1986.

[53] G. Huiskamp, A. Van Oosterom, J. M. De Bakker, and R. Coronel, "The depolarization sequence of the human heart surface computed from body surface potentials: confrontation with invasive measurements," in *Electrocardiology'88*, H. Abel, Ed.: Elsevier Science, Amsterdam, 1989, pp. 35-9.

[54] R. Modre, B. Tilg, G. Fischer, F. Hanser, B. Messnarz, M. Seger, M. F. Schocke, T. Berger, F. Hintringer, and F. X. Roithinger, "Atrial noninvasive activation mapping of paced rhythm data," *J Cardiovasc Electrophysiol*, vol. 14, pp. 712-9, 2003.

[55] A. Van Oosterom and G. Huiskamp, "Spatio-temporal constraints in inverse electrocardiography," in *Biomedical and life physics*, D. Ghista, Ed.: Vieweg, Wiesbaden, 1996, pp. 203-314.

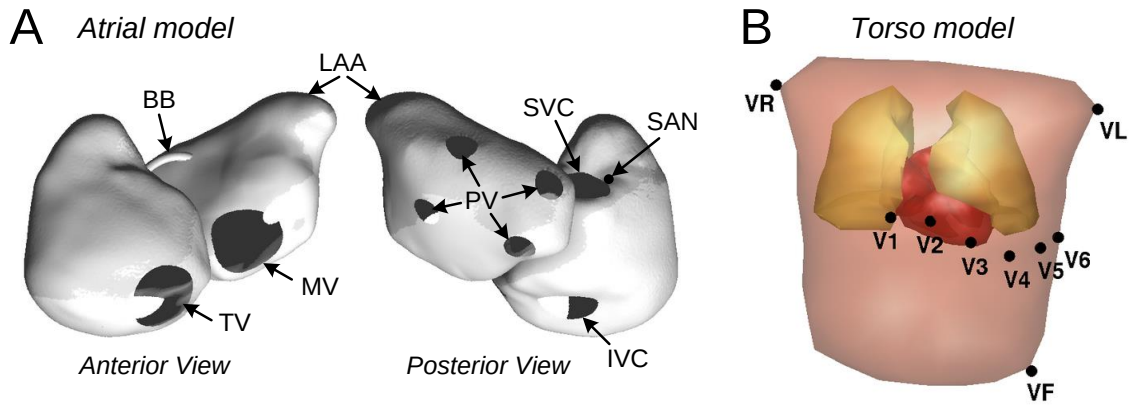

Figure 1: Geometry of the models representing atria and body surface. *Panel A*: Geometry of the atrial model as seen from an anterior view (on the left) and from a posterior view (on the right). The major anatomical details shown, included those blocking propagation: the tricuspid valve (TV), the mitral valve (MV), the inferior vena cava (IVC), the superior vena cava (SVC), and the pulmonary veins (PV). In addition, the location of the sino-atrial node (SAN), the Bachman's bundle (BB), and the left atrium appendage (LAA) are indicated. *Panel B*: Geometry of the compartmental torso model (nearly frontal view) including the atria, the ventricles and the lungs. The positions of the 9 ECG electrodes as used in the standard 12-lead system are indicated; V_1–V_6 are the precordial leads; V_R (right arm), V_L (left arm) and V_F (left foot) are the limb leads.

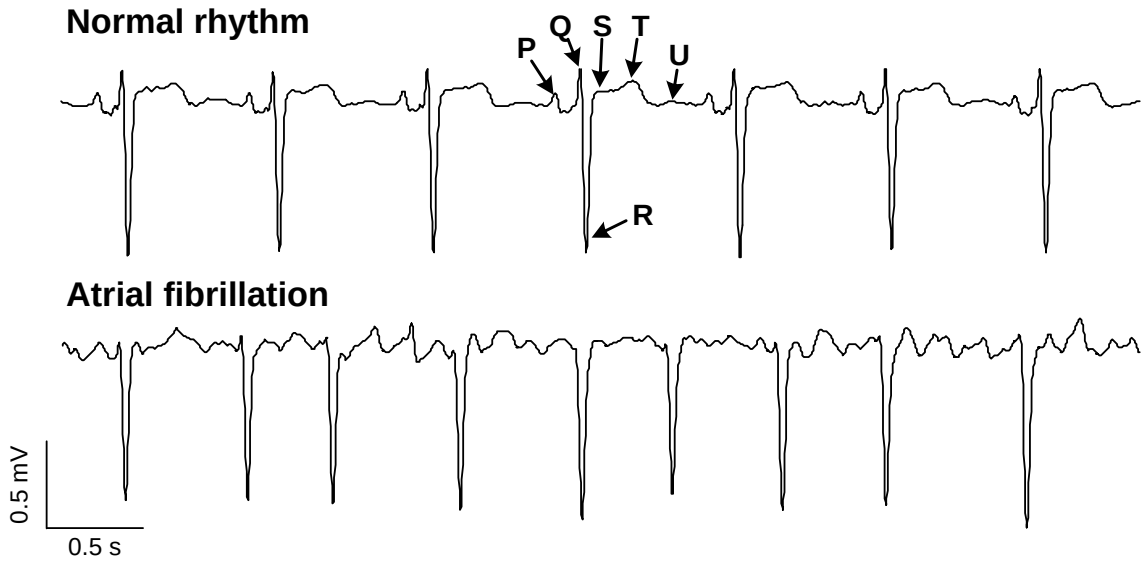

Figure 2: Examples of the ECG as observed on lead V_1. *Upper trace*: signals during normal rhythm. The nomenclature of the P, Q, R, S, T and U waves is as indicated. These relate to the depolarization of the atria (P), the depolarization of the ventricles (QRS) and the repolarization of the ventricles (TU). *Lower trace*: signals during atrial fibrillation.

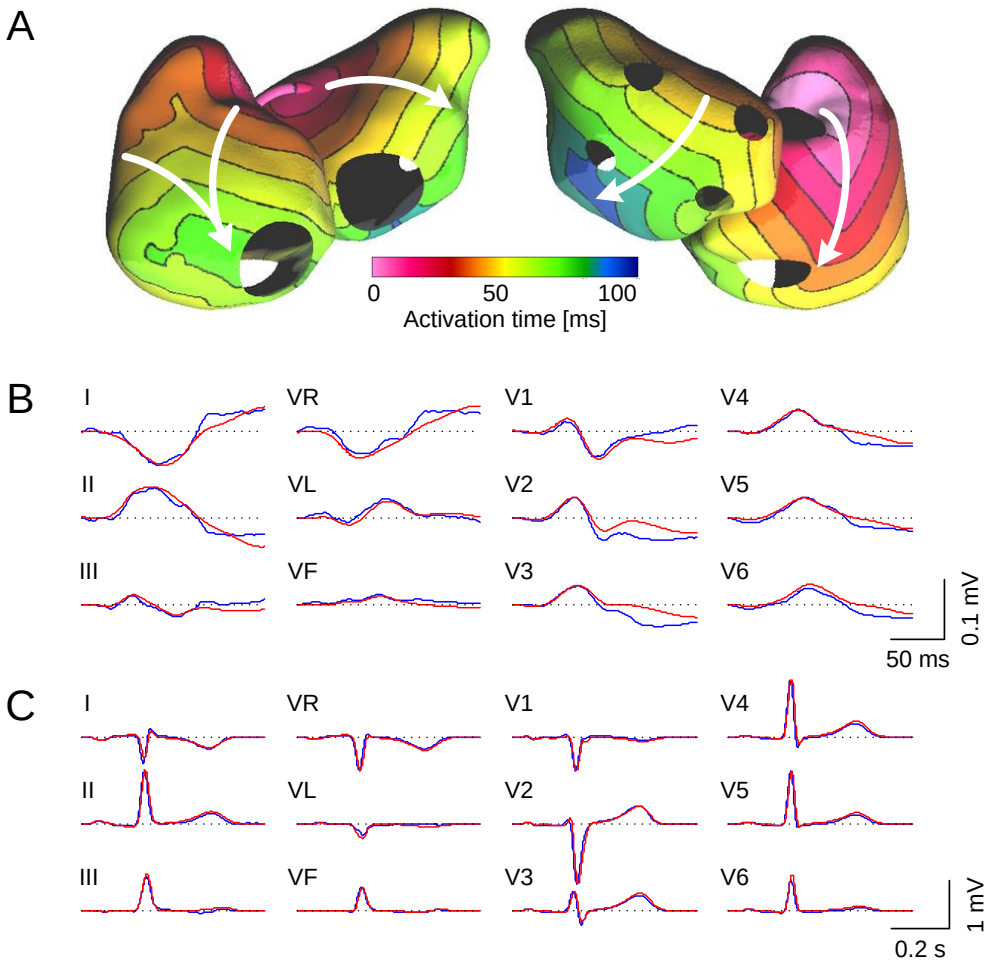

Figure 3: Normal activation of the heart (sinus rhythm) on the atrial surface and as represented in the standard 12-lead ECG. *Panel A*: Propagation of the excitation wave in the atria; isochrones drawn at 10 ms intervals. The wave front is initiated at the sino-atrial node and propagates from the right to the left atrial tissue, as indicated by the arrows. Atrial activation terminates 108 ms after its initiation in the left atrial wall below its appendage, where three wave fronts converge. *Panel B:* P waves shown in the standard layout of the 12-lead ECG. Reference data, from clinical ECGs (blue curves), are shown as well as P waves (red curves) simulated by the model. The simulated P waves resulted from slight adjustment (inverse procedure) of the timing of the transmembrane potentials generated by the atrial activation model. *Panel C*: Complete ECG featuring the PQRST waves. The simulated ECG (red curve) was obtained from a heart model including atria and ventricles. The depolarization and repolarization times of the ventricles were derived from an inverse procedure aimed at fitting the simulated potentials to the measured, clinical ECG (shown in blue). Note that here, as throughout this paper, the signals of the limb leads are shown in an un-augmented scale; this puts them on an equal footing with the other, so-called unipolar, leads.

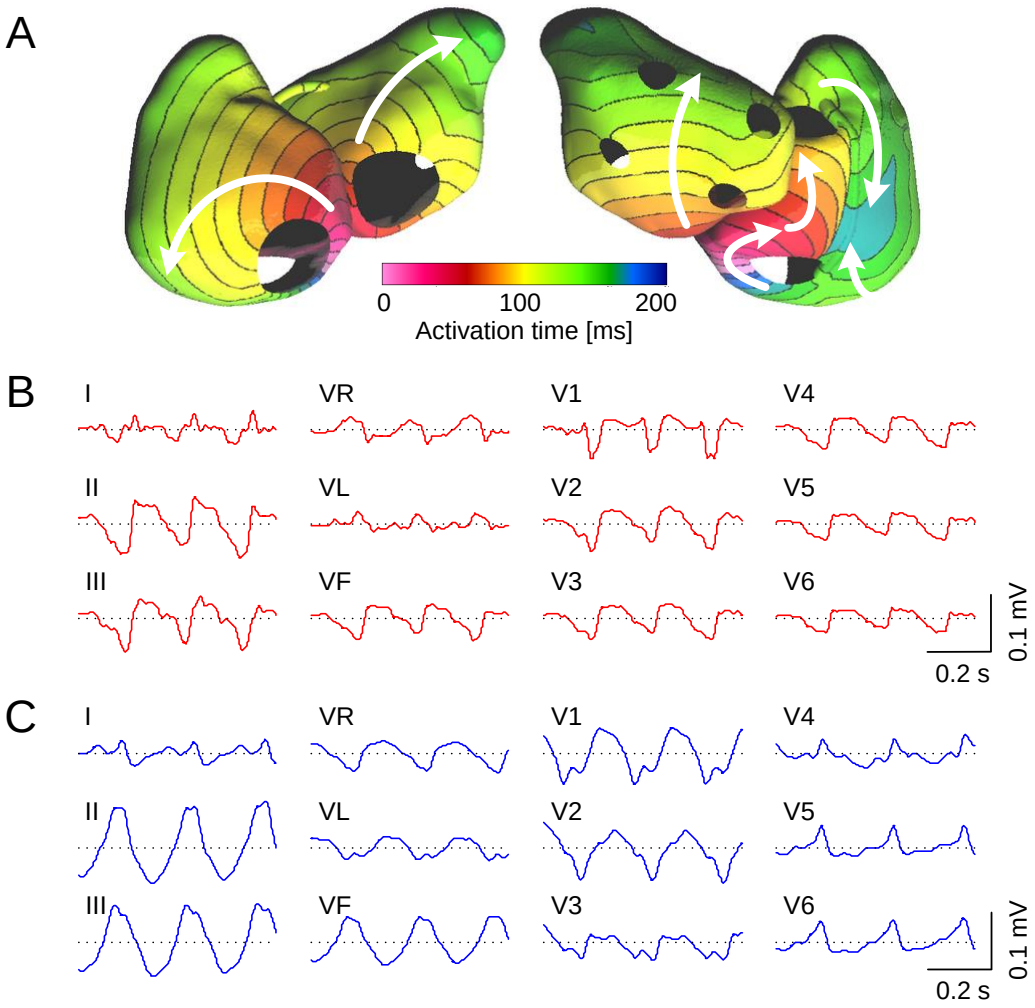

Figure 4: Activation sequence and standard 12-lead ECG during atrial flutter. *Panel A*: Pathway of the reentry represented by isochrones drawn at 10 ms intervals. The circuit encircles clockwise the superior and inferior vena cava, and the crista terminalis, where a functional block occurs. The cycle length is 195 ms. *Panel B*: ECG during 3 cycles resulting from the simulated atrial flutter. *Panel C*: Example of a clinical ECG during typical atrial flutter, included for the sake of illustration. The segment shown was extracted from a (long) TQ interval in which the ventricular activity was silent. Here, no attempt was made to fit the data produced by the model to the clinical signals.

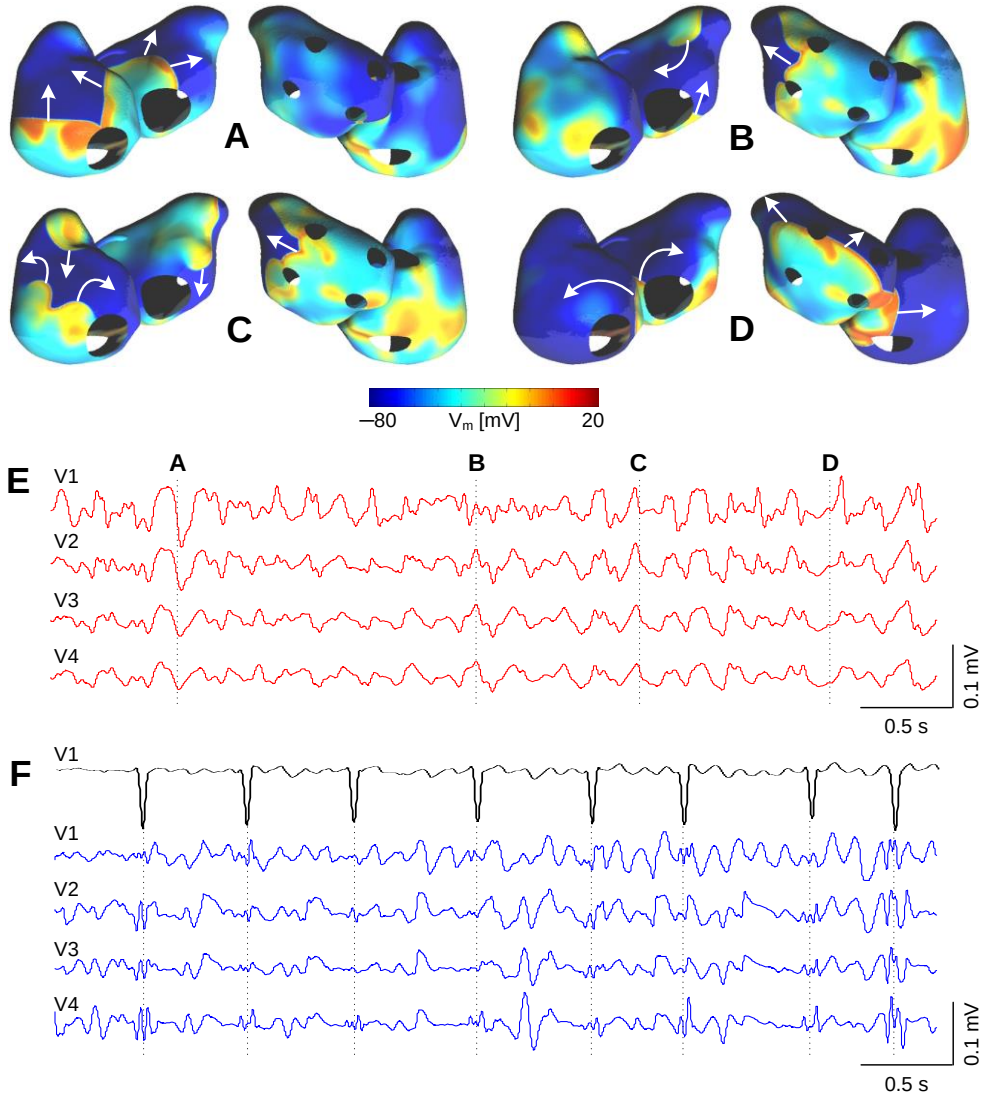

Figure 5: Dynamics of AF as observed from the atrial surface and from the precordial leads of the standard ECG. *Panels A–D*: Snapshots of the wavelet dynamics during simulated AF. The transmembrane potential (V_m) is color-coded, blue and orange/yellow representing resting and excited tissue, respectively. The arrows indicate the direction of propagation of the wavelets. *Panel E*: ECG (leads V_1–V_4, red curves) during simulated AF. Dashed lines indicate the times of the corresponding transmembrane potential maps shown in panels A–D. Note that the modeling approach permits the display of these signals in a manner that is uncontaminated by the electrical activity of the ventricles. *Panel F*: Example of clinical ECG recorded during AF (leads V_1–V_4, blue curves). In order to facilitate the comparison with the simulated signals, a QRST cancellation algorithm was applied to the clinical signals. The recorded signal of lead V_1 prior to QRST cancellation is shown in black as a reference.

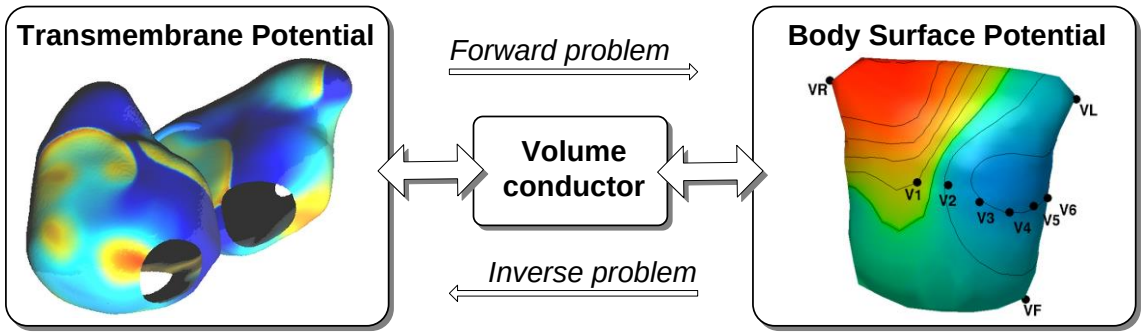

Figure 6: Schematic description of the elements linking atrial source strength and potentials observed on the thorax. *Left panel*: Geometry of the atrial model as seen from an anterior view. The color code represents the instantaneous distribution of the transmembrane potentials acting as the (EDL) strength of the atrial current source. *Middle panel:* representation of all volume conduction effects, including source point-field point relationships and inhomogeneities of the electric conductivities at the torso boundary, atrial and ventricular cavities and lungs. *Right panel*: Geometry of the torso surface (near frontal view). Color-coded representation of the body surface potential distribution resulting from the source strength illustrated in the left panel. Color code: red for positive potentials, blue for negative potentials; isopotential lines drawn at 20 μV intervals.

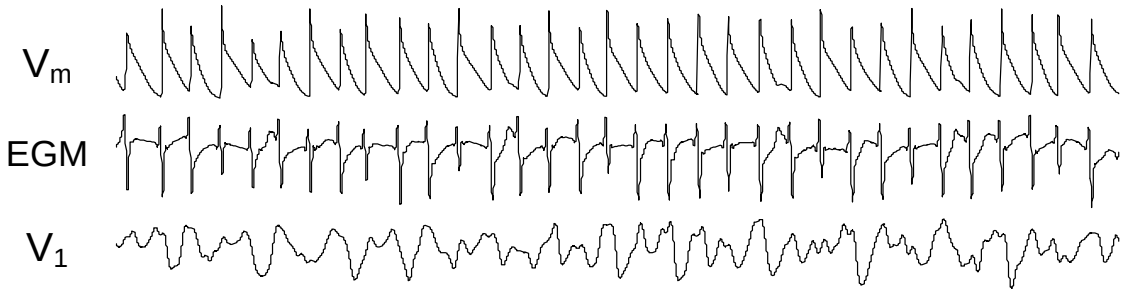

Figure 7: Wave forms computed during 5 seconds of a simulated AF episode. *Upper trace*: transmembrane potential at the atrial node closest to the position of the electrode of lead V_1; *Middle trace*: electrogram at the same atrial node; *Lower trace*: the AF signal of lead V_1 resulting from summing the contributions of all (1300) nodes on the atrial surface.

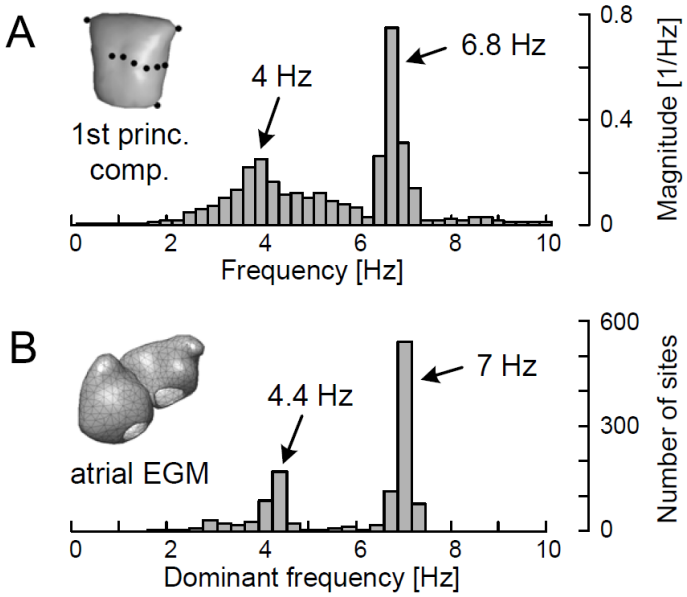

Figure 8: Comparison of the frequency content of body surface potentials and atrial electrograms. *Panel A*: Power spectral density of the first principal signal component (having unit power). *Panel B*: Histogram of the dominant frequencies of the 1300 atrial electrograms (EGM) evenly distributed over the entire atrial surface.

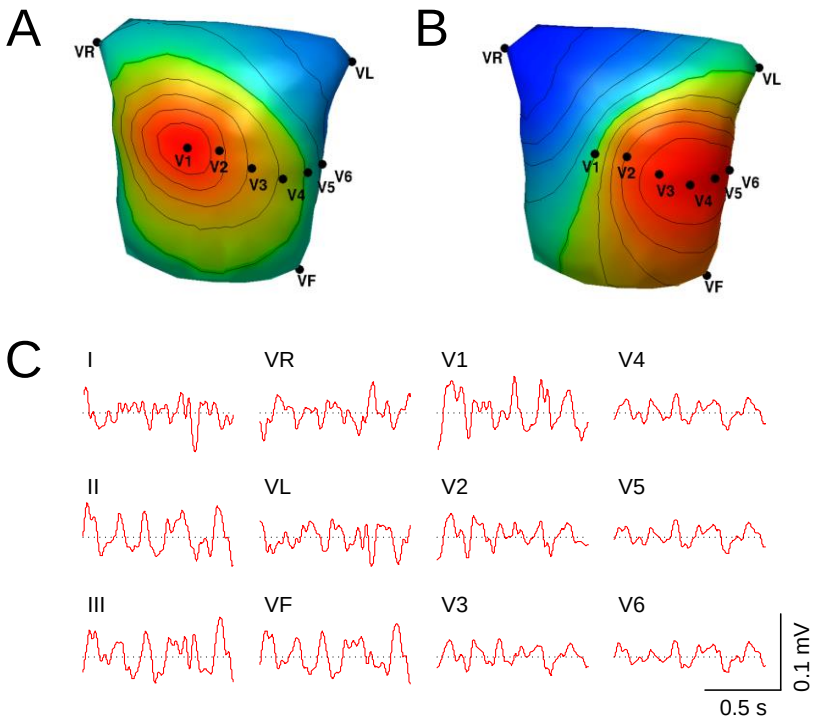

Figure 9: *Panel A*: Map of the correlation coefficients between a signal segment of AF, lasting 1 s, in lead V_1 and the corresponding signals of all other (299) lead positions on the thorax; iso-correlation lines drawn at intervals of 0.2. *Panel B*: as in Panel A, but now with reference to lead V_4. *Panel C*: Wave forms in the 12-lead ECG during the simulated AF episode. Note that the wave forms in leads V_4, V_5, and V_6 are very similar, and, apart from a different sign, also similar to that in lead V_R.